Study of tetrahedral metal nanoparticle arrays produced by nanosphere lithography

Sophia Linssen-Pitsaros

July-September 2022

Contents

0.1 Introduction 2
0.2 Radio-Frequency Sputter Deposition 2
0.3 Grazing-Incidence Small-Angle X-Ray Scattering 3
0.4 Methods 5
0.4.1 Sample Preparation 5
0.4.2 Monolayer Production 5
0.4.3 Sputter Deposition 6
0.4.4 Sonication 6
0.4.5 Measurement 7
0.5 Results & Analysis 7
0.5.1 Polystyrene Monolayer 7
0.5.2 GISAXS & SEM 12
0.6 Conclusion 14

0.1 Introduction

Nanosphere lithography is an in-expensive method used to fabricate homogeneous, close-packed nano-scale structures such as 2D nanoparticle arrays. Nanostructures have been found to exhibit correlation between size and property with their properties being different to their bulk counterpart [1] which raises questions such as what the causes of these properties are and the functional materials that could spawn from this knowledge. The size-dependent properties include, for example, optical [2], magnetic [3] and catalytic [4]. Studies into the applications of these properties include biosensors [5], chemical sensors [6], data storage [7]. Ongoing research is being conducted to investigate structure-property relationships for a variety of nanostructures with different materials, nanoparticle shape and pattern and the techniques used to make them. One particular technique being explored is nanosphere lithography [8]. Nanosphere lithgraphy is a bottom-up approach that relies on the self-assembly [9] of a nanosphere monolayer that is used as a template to produce a 2D nanoparticle array. Unlike top-down techniques, nanosphere lithography is able to fabricate with high-throughput nanoparticles with dimensions below 10nm [9]. Various method exist to create the nanosphere template that include drop casting [10], spray coating [11], spin coating [12], and Langmuir-Blodgett coating [13], [14].

In this paper, tetragonal metal nanoparticle arrays are fabricated and studied. Different techniques (drop casting, spin coating and angled Langmuir-Blodgett coating) are tested using nanospheres with a variety of sizes, to fabricate a close-packed, homogeneous monolayer. The project has a particular focus using spin coated templates made with polystyrene nanospheres of diameters below $1000nm$. The templates are sputtered onto with silver then ultra-sonicated to remove the nanospheres. The resulting 2D silver nanoparticle is measured and imaged using grazing-incidence small-angle x-ray scattering and scanning electron microscopy respectively to extract information about the distances between silver nanoparticles, the monolayer coverage and thickness.

0.2 Radio-Frequency Sputter Deposition

Sputter deposition is an industrial standard technique that has been widely used to fabricate thin-layer coatings since the 1800s. It is a physical vapour deposition technique which deposits the coating material atom-wise onto the substrate. The process uses a plasma to eject sputter atoms from a target material towards a substrate. It can produce uniform, dense, deformity-free coatings with high-throughput and reproducibility and provides flexibility to specify coating thickness and substrate/target material. In general, the sputter system is contained within a vacuum chamber at a working pressure of $10^{-6}mbar$. The chamber is filled with argon gas, an inexpensive inert gas that won't react with the target or substrate. The substrate is placed on top of an anode and the target material is placed onto a cathode directly above the substrate (Figure 1).

With a voltage applied across the anode and cathode, the resulting electric field strength is sufficiently large enough to cause free electrons to collide with high enough energy to ionise argon gas molecules. The further release of electrons, referred as a Townsend avalanche, is triggered. Positive gas ions travel to the cathode following the external electromagnetic field and stimulating the secondary release of electrons from the cathode. The magnetron localises secondary electrons by the target. The energetic gas ions collide with atoms from the target material. The ion momentum

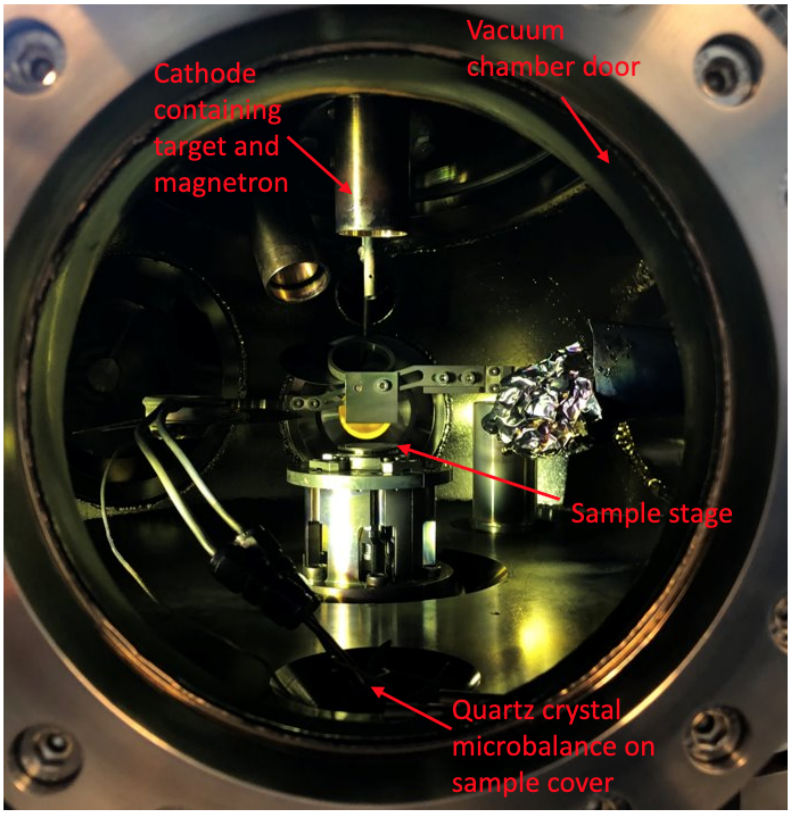

Figure 1: RF magnetron sputter chamber with the cathode containing the magnetron and target material in line-of-sight of the sample stage that is connected to an anode.

is transferred to the targets surface atoms which gain sufficient energy to overcome the surface binding energy. The released target atoms travel towards the substrate, creating a layer.

Compared to the other deposition methods (direct current (DC), radio-frequency (RF) magnetron, Pulsed DC and alternating current (AC) sputtering), RF magnetron sputtering has the highest sputter rate and also allows for the use of insulator, semiconductor and polymer targets [15]. The oscillatory motion of the electrons due to the high-frequency alternating voltage increases the ionisation of argon atoms and therefore increases sputter rate. The high-frequency alternating voltage continuously neutralises positive ions on the target to prevent a build-up of positive charge on the target and the termination of the process. A magnetron is used to localise the electrons to the target surface, increasing the plasma density and therefore increasing deposition rate.

0.3 Grazing-Incidence Small-Angle X-Ray Scattering

GISAXS is a non-invasive, non-destructive technique used to measure nanostructures at surfaces, or interfaces, probing information such as structure size, shape and lateral distance between adjacent structures. It relies on the reflection of incident light to produce a 2D intensity pattern (Figure 2). In the case that the sample being measured is homogeneous, all incident light would be scattered by the same angle resulting in a dot on the 2D detector. Dispersity in size, shape and distances

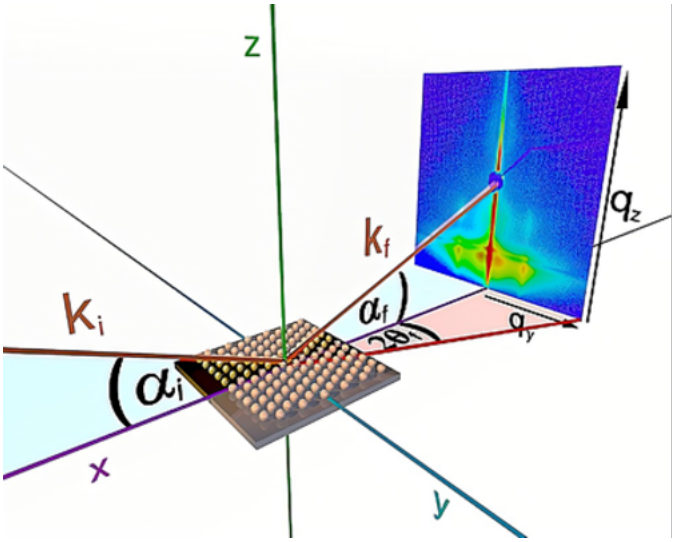

Figure 2: GISAXS scattering set-up [16]. The incoming x-ray beam has a wave vector k_i (lies in x-z plane) and an incident angle to the sample surface α_i. The scattered x-ray beam has a wave vector k_f (lies in x-z plane) and an incident angle to the sample surface α_f. The intensity pattern is in reciprocal space. Beam stoppers are positioned to block the high intensity specular and direct beam from reaching the detector, preventing detector saturation and damage.

between structures will cause the incident light to be scattered by different amounts via different mechanisms [17].

The intensity patterns contain two main features:

- Specular Peak: Produced by light scattered when the incident angle α_i equals angle of reflection α_f.
- Yoneda Region: Yoneda region contains a peak where the incident angle is equal to the critical angle of the material. This region arises from off-specular scattering ($\alpha_i \neq \alpha_f$) and contains information about the morphology of the sample.

Unlike other techniques, GISAXS gives the ability to examine specific depths inside the material by choosing incident angles that fulfill the specular scattering condition. In-plane inter-particle distance and morphological information can be probed by off-specular scattering. The technique can be carried out ex-situ, in-situ and real-time, providing the opportunity to study morphological evolution during processes such as sputter deposition [18].

The intensity depends on the interference function, representing the surface topology, and the form factor which models object shape [15]. A polydispersive (variation in object shape and size) nanostructured surface will cause a smearing of the form factor. Information on object height can be extracted from intensity along the q_z direction.

$$q_y = \frac{2\pi}{d} \tag{1}$$

By taking a vertical cut (detector cut [15]), information such as average nanoparticle height and layer thickness can be calculated. Horizontal (Yoneda) cuts provide insight into average particle size and inter-particle distances. Inter-particle distance, d, can be calculated by finding the q_y value of the Yoneda cut maxima and using eq.1.

0.4 Methods

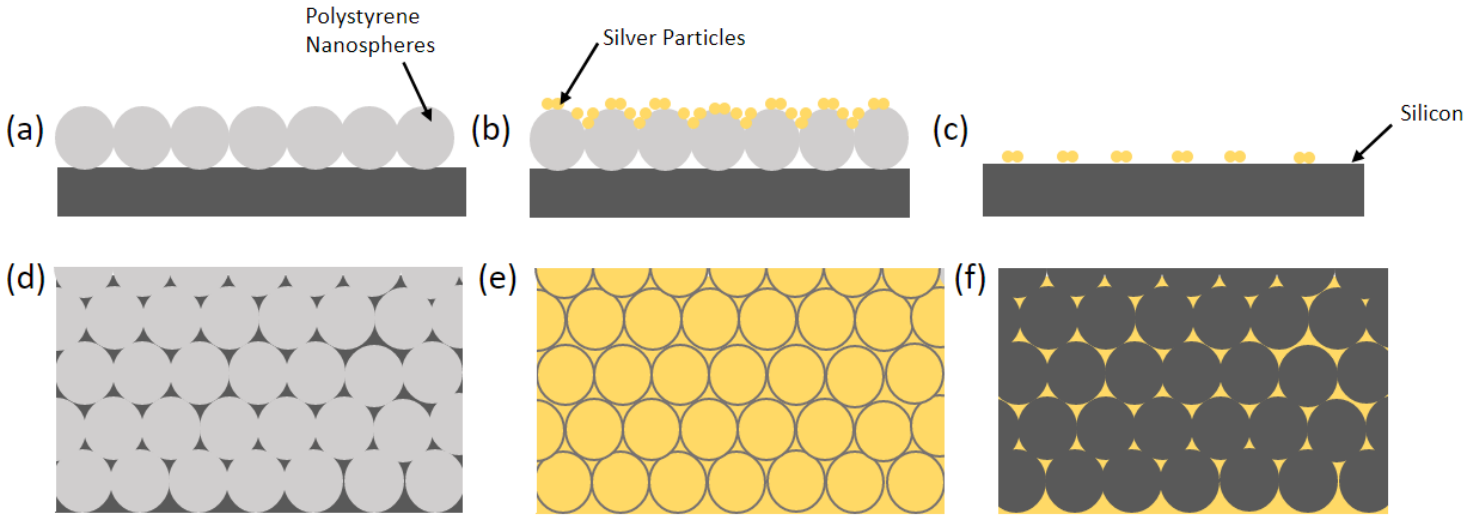

Figure 3: Overview of fabrication of silver nanoparticle array. Side view of silicon wafer (top row). Aerial view of silicon wafer (bottom row). (a) & (d) polystyrene nanosphere monolayer. (b) & (c) polystyrene monolayer sputtered with silver. (c) & (e) Silver nanoparticle arrays remaining after polystyrene monolayer removal.

0.4.1 Sample Preparation

$11 \times 15mm^2$ boron-doped silicon wafers were cleaned using a Pirahna solution (similar to method in [19]) to remove organic contaminants on the surface and to cause the surface to become more hydrophilic. The wafers were stored for the maximum duration of a week in a pure water bath. Before use, substrates were rinsed with de-ionised water and dried with nitrogen.

0.4.2 Monolayer Production

The aim was to fabricate a close-packed, uniform monolayer with high coverage of polystyrene nanospheres (Kisker Biotech GmbH and Co. KG, Germany). The polystyrene solutions (PPs) used contained nanospheres with diameters 4μm, 3μm, 2μm, $1011nm$, $381nm$, $194nm$, $48nm$ & $25nm$. Spin coating, Langmuir-Blodgett coating and drop casting were tested. All resulting samples were imaged with an optical microscope.

Spin Coating

Spin coating was performed in two steps. The initial spin was performed at low speed with gradual acceleration up to maximum speed over a long time. The aim of this was to spread the solution over the substrate. The second spin step was higher speed and acceleration for a short time period. This would, in principle, cause the clusters to break into a monolayer, roll bi-layer particles into gaps and expel any excess material. $50\mu L$ of $4\mu m$ PPs solution was spun varying individually the speeds ($100RPM$-$250RPM$) and time duration ($60s$-$600s$) of the first step and the acceleration of the spin coater (1-9). The second step speed was set to $1000RPM$, acceleration 9 and the time durations were tested in the range $10s$-$60s$.

To investigate the effect of a surfactant on spin coating results, methanol and ethanol were separately mixed with the polymer solution in specific ratios (See 19). The solutions created were made up of $10, 20, 30, 40$ and 50 per cent surfactant with the remaining percentage being polymer solution with nanosphere diameters above $1011nm$. These samples were all spin coated with step 1: 160RPM, 9 acceleration & 120s and step 2: 1000RPM, 9 acceleration & 10s.

Drop Casting

Methanol-polymer solutions were used for drop casting. The different volumes of solution drop casted included $25, 35, 40, 50\mu L$. This was performed for 3 and $4\mu m$ polystyrene solutions for all the methanol amounts between 10% and 50%.

Langmuir-Blodgett Coating

The Langmuir-Blodgett coating technique uses an air-water interface to form a close-packed colloid monolayer which can be transferred onto a substrate by an angled lifting of the substrate from under the monolayer. Subsequent drying involves positioning the substrate at an angle to encourage optimal evaporation of solvent [14]. Between 100 and $300\mu L$ of surfactant-polymer solution (separately using ethanol and methanol) was applied on the surface of de-ionised water in a flask. The substrate was dipped and removed at an angle as to collect the surface layer of polystyrene and was positioned at an angle to dry for 24 hours. This was performed using 10%-50% methanol for 3 and $4\mu m$ colloids.

0.4.3 Sputter Deposition

Spin coated samples produced with colloids of $50nm$ diameter were coated with silver (Ag) in a radio-frequency magnetron sputter chamber for 1000s at a $10^{-6}mbar$ working pressure. A mask was positioned to only sputter half the sample area. Before deposition, the sample was covered with a quartz crystal micro-balance to measure the rate of deposition (0.11A/s).

0.4.4 Sonication

The sputtered sample was placed in a sonication bath for 15 minutes to remove the polystyrene nanospheres leaving a silver nanoparticle array. Once sonicated, samples were dried with nitrogen.

0.4.5 Measurement

The $50nm$ sample was measured using GISAXS before and after the polystyrene was sonicated off the wafer leaving the silver nanoparticle array. A GISAXS y-direction scan was conducted which scanned across the wafer so as to measure the silver sputtered area, the non- silver sputtered area and the interface between them. Scaning electron microscopy was used to image the sample after sonication. GISAXS data was analysed using DPDAK. Detector distance was calculated by calibrating the direct beam images with the calibrant image. The calibrant used was silver behenate. Detector distance for the GISAXS of the $50nm$ sample was $4050mm$.

0.5 Results & Analysis

0.5.1 Polystyrene Monolayer

Overview

Langmuir-Blodgett coating appeared to be limited in working well for only colloids above $1011nm$ diameter. Smaller colloids (below $1011nm$), in the presence of a surfactant, were not able to produce monolayers on the water surface. Spin coating was used to create monolayers consisting of the small diameter colloids. The $48nm$ diameter colloids produced the most homogeneous, close-packed monolayer compared with other small colloids.

Spin Coating

Spin coating, performed with $4\mu m$ nanoparticles without the use of a surfactant, produced inhomogeneous polystyrene films consisting of sparse clusters in the centre of the film and double layers on the film edge (Figure 4). During the second step of the spin process, a double expulsion of the material on the wafer was observed. The time of the first step was decreased to $120s$ and the time of the second step to $10s$, thus preventing the double expulsion of material and resulting in a centre more densely populated with polystyrene nanoparticles (Figure 4).

Figure 4: $4\mu m$ Polystyrene nanospheres spun with step 1: $150RPM$, ramp 1, duration $600s$, step 2: $1000RPM$, ramp 9, duration $60s$ (Left) and spun with step 1: $160RPM$, ramp 1, duration $120s$, step 2: $1000RPM$, ramp 9, duration $10s$ (Right).

Spinning methanol, mixed with $3\mu m$ and $4\mu m$ polystyrene nanoparticles in the ratios 2:8 and 3:7 respectively, produced the close packed films that contained bilayers. The use of bi-layer templates could be further invesigated in the future as a means to create nanoparticle arrays with more complex shapes. The ramp 6 setting, used for the $3\mu m$ solution with a methanol-polymer ratio 40:60, produced the best monolayer (Figure 5).

Figure 5: Optical microscope image (a) and SEM image (b) of sample made with $3\mu m$ solution with a methanol-polymer ratio 40:60, spun with settings: Step 1, $160RPM$, $120s$, ramp 6; Step 2, $1000RPM$, $10s$, ramp 9.

Spin coating with ethanol-($3\mu m$) polymer solutions was performed using the standard spin setting: step 1, 160RPM, 120s, ramp 6 ; step 2, 1000RPM, ramp 9, 10s. For all surfactant-polymer ratios, this resulted in films that contained homogeneous monolayers with some areas containing bi-layers (Figure 6). Ethanol is a less toxic, cheaper surfactant; therefore, it could replace methanol.

Spin coating, tested using 25nm diameter polymer nanospheres, caused all the material to expel from the film, at standard spin setting, leaving an inhomogeneous distribution of nanoparticles (Figure 8). Using an optical microscope on this sample revealed that the film was empty except for a few layers of nanoparticles arranged in a ring, showing as a coloured ripple effect (Figure 7). The 48nm colloids were mixed with ethanol, filtered and spun at 2000RPM, ramp 9 for 30s. The samples showed a homogeneous brown coloured layer with a few domains with multilayers and contaminants (Figure 9). The brown colour is due to thin film interference and corresponds to a 100nm monolayer.

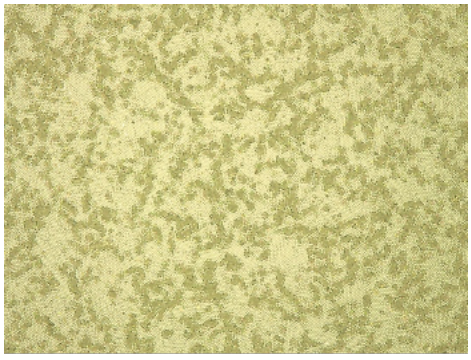

Figure 6: Spin coated sample using ethanol-($3\mu m$) polymer solution in the ratio 40:60.

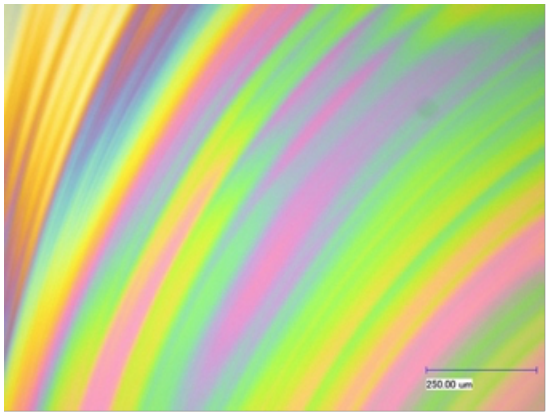

Figure 7: Optical microscope image of sample made with $25nm$ solution with a methanol-polymer ratio 1:1, spun with settings: Step 1, $160RPM$, $120s$, ramp 6; Step 2, $1000RPM$, $10s$, ramp 9.

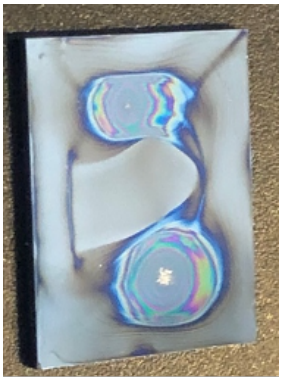

Figure 8: Sample made with $25nm$ solution with a methanol-polymer ratio 1:1, spun with settings: Step 1, $160RPM$, $120s$, ramp 6; Step 2, $1000RPM$, $10s$, ramp 9.

Drop Casting

Drop casting was tested for 3 and 4 micrometers polystyrene methanol solutions of different concentrations. The resulting film consisted of close packed bi-layers, and some sparse domains of monolayers. Some films showed a ripple effect (Figure 10), implying the presence of the coffee ring effect. This could be caused by the termination of motion of the edge of the solution droplet due to surface tension. Since the edge of the droplet is exposed to more air than the centre, the methanol at the edge will dry faster. To compensate for this, a flow of solution (methanol and polymer) to the edges arises, therefore reducing the amount of polymer in the centre. When fully dry, there is a ring concentrated with polymer particles. Since the substrate is hyrophilic (from pirahna cleaning), the static edge of the droplet will be near the center of the droplet creating a stain [20].

The films, fabricated using angled Langmuir-Blodgett coating, had large areas of uniformly densely packed monolayers. The most successful samples has concentrations 20:80 and 50:50. The use of surfactants has been known to improve the mechanical stability [13]. When a solution of surfactant mixed with polymer is put onto the surface of water, the surfactant will lie on the air-water

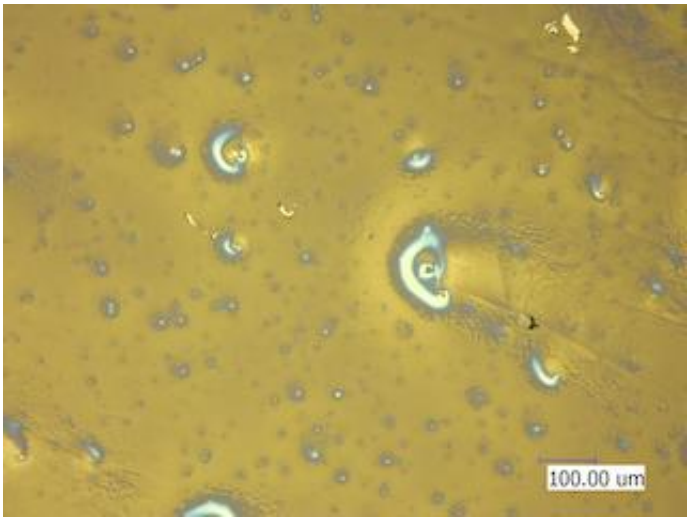

Figure 9: Spin coated sample using ethanol-($48nm$) polymer solution.

Figure 10: Photo of sample made with $4\mu m$ solution with a methanol-polymer ratio 10:90

interface and will cause the polymer particles to push together, creating a closepacked monolayer on the water. The surfactant will reduce surface tension, which aids the movement of spheres on the surface to configure into a monolayer [14]. The advantage of this method is the minimal number of parameters that need to be varied to create a closepacked, homogeneous monolayer.

Figure 11: $4\mu m$ Polystyrene nanospheres produced by angled Langmuir-Blodgett coating using a 2:8 ratio of methanol to polystyrene solution. Optical microscope image (left) and photo of sample (right)

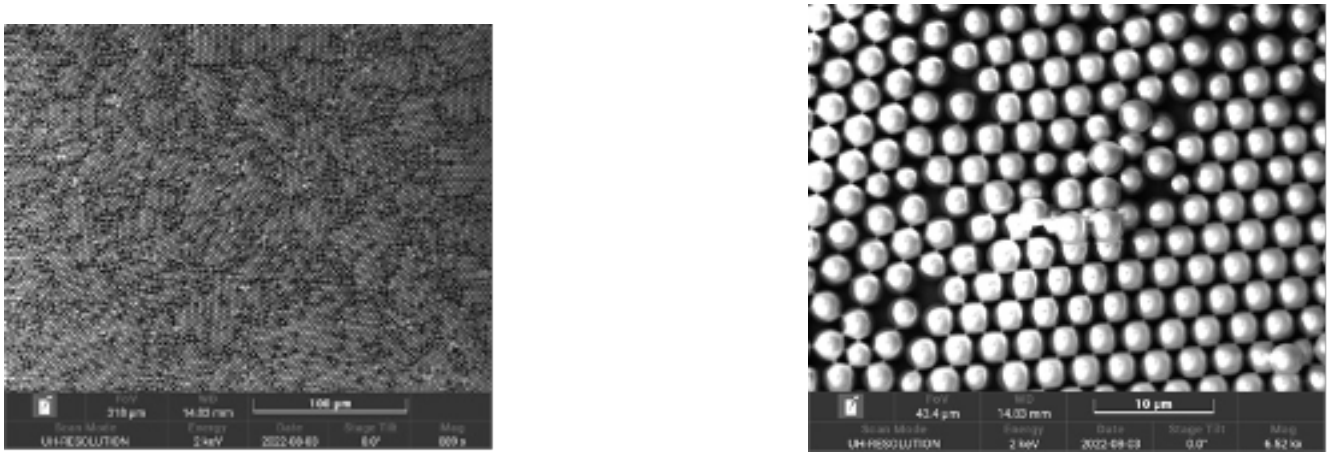

Figure 12: SEM images for $4\mu m$ Polystyrene nanospheres produced by angled Langmuir-Blodgett coating using a 2:8 ratio of methanol to polystyrene solution.

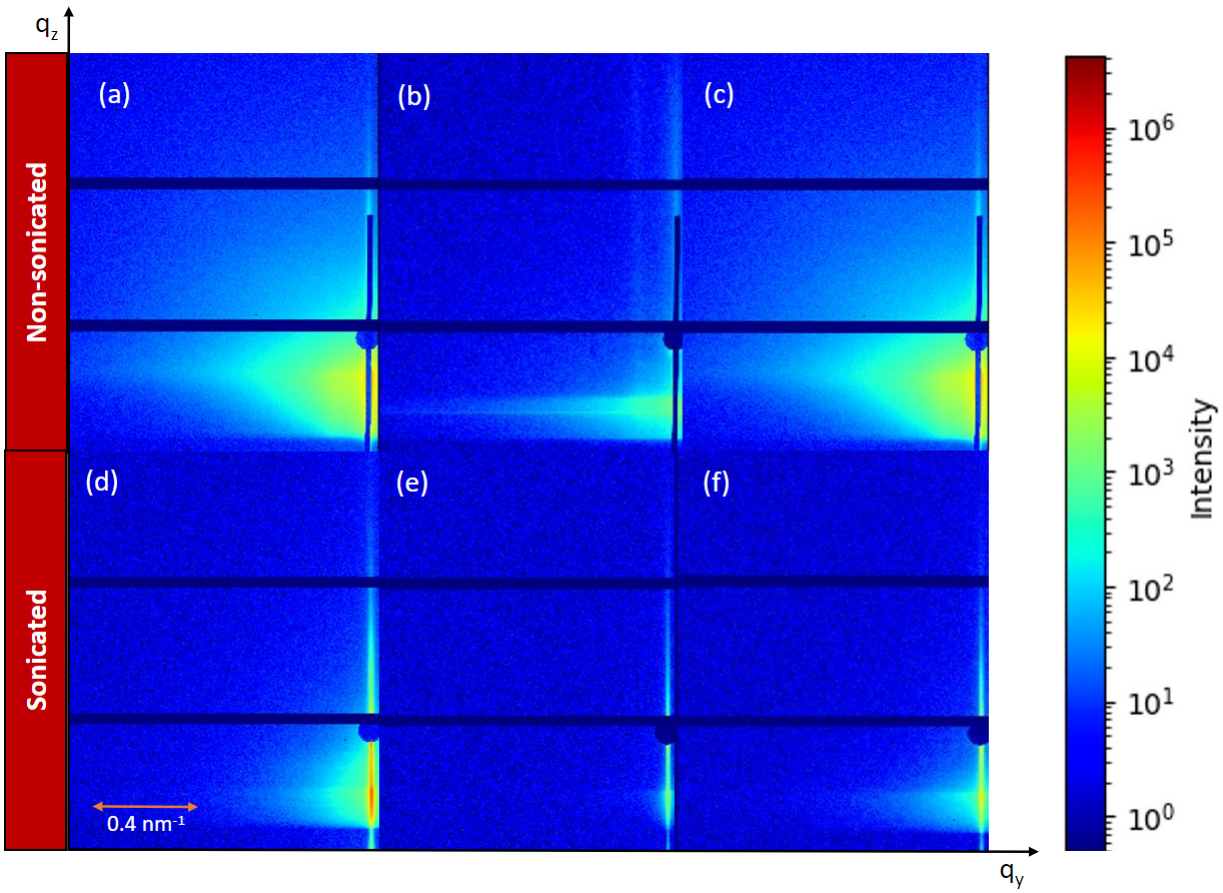

Figure 13: 2-Dimensional GISAXS patterns taken from y-scan raw data. (a), (b), (c) are the scans of the silver sputtered on the polymer monolayer half of the wafer, the monolayer side of the wafer and the interface between the two respectively.(d), (e), (f), are the scans of the silver nanoparticle array half of the wafer, the silicon after the monolayer was sonicated off and the interface between the two halves respectively.

0.5.2 GISAXS & SEM

There are two possibilities for which distances are probed by GISAXS for the (non-sonicated) silver sputtered polystyrene (PPS) monolayer (Figure 14). For small clusters of silver particles present on the polymer nanospheres (i.e. silver caps), the distance probed by GISAXS could be that between individual silver atoms or that between the silver clusters. To investigate this, log graphs of the Yoneda linecuts for the plain PPS monolayer, the silver sputtered PPS monolayer and the Ag nanoparticle arrays left after sonication of the PPS layer were produced (Figure 18). The average distances probed for the polystyrene monolayer, Ag sputtered on the polystyrene monolayer and the Ag nanoparticle array resulting from sonicated sputtered monolayer were: $D_{PPS} = 41.0nm, D_{Ag} = 50.3nm$ and $D_{Ag,nano} = 82.1nm$ (calculated with 1). The value of the distance probed for silver sputtered on a polymer monolayer is approximately equal to the diameter of the colloids which suggests that the distance probed is that between the silver caps present on the nanospheres. SEM images of the sonicated sample exhibit areas of silver covered polystyrene nanospheres. Higher resolution SEM images would be required to examine whether silver caps can be observed.

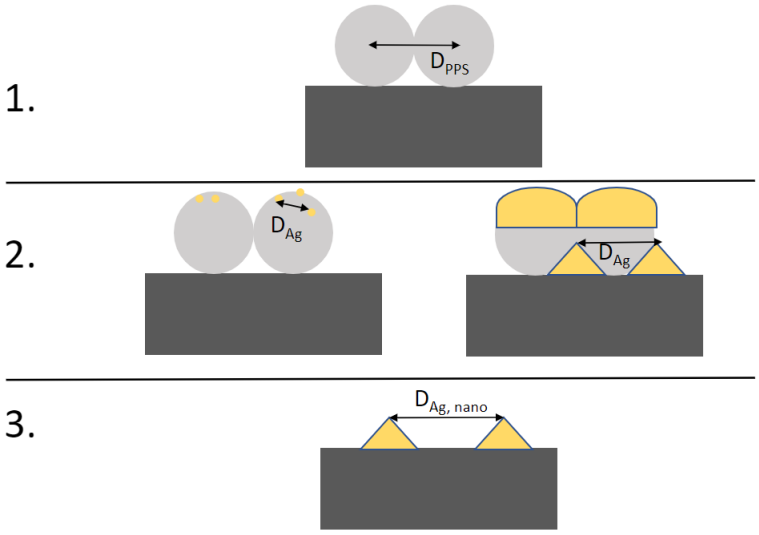

Figure 14: Illustration for the different distances probed in GISAXS for (1) PPS monolayer on silicon, (2) silver sputtered onto PPS monolayer on silicon and (3) sonicated silver sputtered onto PPS monolayer

When the silver sputtered PPS monolayer is sonicated (removal of polystyrene template), the broad peak decreases to lower q_y values (Fig.13d) than the value of the silver sputtered PPS monolayer (Fig13a). This suggests the distances between object centres is larger for the Ag nanostructures left after sonication compared with the non-sonicated silver sputtered PPS monolayer. This can also be seen in the increase in average distances for the Ag on PPS layer compared with the pure PPS monolayer. Unlike polystyrene nanospheres, which have 6 equidistant neighbour particles, the silver nanoparticles have 3 short distant neighbours and have 4 long distance neighbours. Therefore, the most prominent in-plane particle distance will be longer (as seen in results) for the silver nanoparticles compared with capped polystyrene nanospheres.

The distance between the nanoparticle arrays is much larger than that of the polystyrene nanospheres, therefore, it is implied that there is no templating effect [17].

Smearing around the Yoneda region of Fig.13e could hint at the presence of leftover polystyrene, or other contaminants, on the silicon surface. This confirms the incomplete sonication of the sputtered monolayer. Traces of leftover polystyrene nanospheres are visible on the SEM images Fig.16a, d, e, f.

The critical angle of silicon found from the vertical line cut, $\alpha_{c,linecut} = 0.135°$, was lower than the reference value for silicon probed at energy $11850eV$, $\alpha_{c,ref} = 0.151°$ [21]. This difference could originate from the silicon having a different density to the reference density, the existence of organic, PPS, or oxide layers on the silicon, or the detector incident angle being incorrectly set. The detector distance was estimated to be 3.9m but using the calibrant images, it was calculated to be 4.05m. The incident angle should be 0.366 deg as opposed to the estimated 0.38 deg. This could have caused a systematic error for the vertical linecuts.

In Fig.13b, there are two horizontal peaks: the top is the critical angle for silicon and the bottom is the critical angle for the polymer; the lower horizontal peak is stronger, implying that there is a high coverage of polymer on the silicon. Evanescent waves in the silicon polymer interfere and produce a smeared intensity between the silicon and polymer peaks. Bragg rods [17] are visible suggesting the presence of a monolayer on the silicon.

There is an asymmetry visible in the linecut interface between the plain polystyrene monolayer and the silver sputtered polystyrene monolayer (Fig.15c). The symmetry of all other linecuts implies this feature is unique to only this interface. This result could indicate the existence of an asymmetry in the sputter coating of the masked atoms at the interface. When a mask is placed over the centre of a wafer, the sputter atoms in the atmosphere of the chamber could, in principle, sputter the sides of masked atoms exposed to the air. Placing the masks overhanging the edges of the wafers could reduce probability of sputter atoms reaching the masked atoms. The asymmetry of the silver coating on the nanosphere would lead to scattering in different directions, therefore creating an asymmetry in the scattering intensity.

Examining the beauty shot taken of the Ag nanoparticle array remaining after sonication (Fig.17), an angled peak is visible on the left hand-side of the image. Similar angled peaks were observed in [22] that were due to the facets of a 3D structure. The cause of the streak in this data could be a result of the facets of the Ag nanoparticles which, theoretically, are tetrahedron shaped. Further investigation into these angles peaks could be done by rotating and measuring the sample. Other facets of the shaped nanoparticles would be expected to show GISAXS intensity streaks of different angles.

0.6 Conclusion

Three coating techniques were explored in order to find a method that will produce homogeneous, close-packed, high-coverage monolayers on silicon with high reproducibility. The techniques were tested for different size particles ranging from $4\mu m$ to $25nm$. A focus was put on the $48nm$ particles and GISAXS measurements were taken for a $48nm$ monolayer. The $48nm$ nanoparticles produced appropriate monolayers when spin coated, whereas the larger nanoparticles produced very good monolayers when using Langmuir Blodgett coating. More time would be required to explore the spin parameters for other small colloids.

Comparison between the GISAXS measurements for the polystyrene monolayer and the Ag nanoparticle arrays helped rule out templating effects since the distances between polystyrene spheres do not coincide with that of the Ag nanoparticles. The comparison between the GISAXS measurements before and after sonication hints to the presence of silver caps positioned on the polystyrene nanospheres and reveals that sonicating leads to an increase in particle distance. The possible reason for this is that the Ag nanoparticles will have more distant than close neighbours compared to silver capped nanospheres, which has 6 equidistant neighbours. This would lead to the average particle distance being larger.

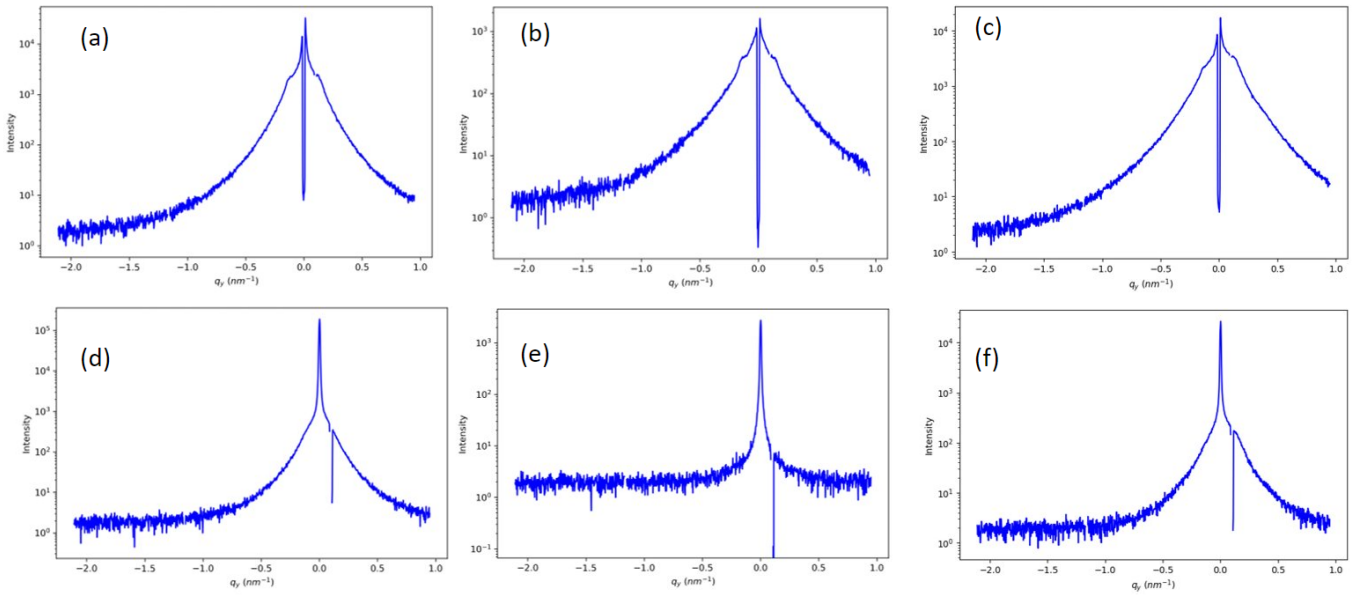

Figure 15: Yoneda linecuts taken from y-scan raw data. (a), (b), (c) are the scans of the silver sputtered on the polymer monolayer half of the wafer, the monolayer half of the wafer and the interface between the two respectively. (d), (e), (f), are the scans of the silver nanoparticle array half of the wafer, the silicon after the monolayer was sonicated off and the interface between the two halves respectively.

The presence of a monolayer is verified by the clear Bragg peaks on the GISAXS taken of the polystyrene monolayer. An asymmetry was observed at the interface between silver covered polystyrene and plain polystyrene. It has been suggested that this is originates from an asymmetry in the silver coverage on the nanospheres. This could be explained by an penumbra effect that occurs when the sputtering particles are able to reach nanospheres under the edge of the mask, therefore coating one side of them. This could be avoided in future work by positioning the masks to hang over the outer edge of the sample substrate.

An angled streak that appeared in the long exposure scan of the Ag nanoparticle array, could be evidence for facets of the theoretically tetrahedral-shaped silver nanoparticles. For future work, more closely packed homogeneous samples of small colloids should be made and measured in GISAXS. The samples should be rotated so the angled streak can be investigated to establish whether it changes position when probing other facets. Work should be done to explore the structure-property relationship of the Ag nanoparticle arrays. This could be done by taking UV-Vis spectroscopy and ellipsometry to measure the optical properties and correlate them with the structural findings.

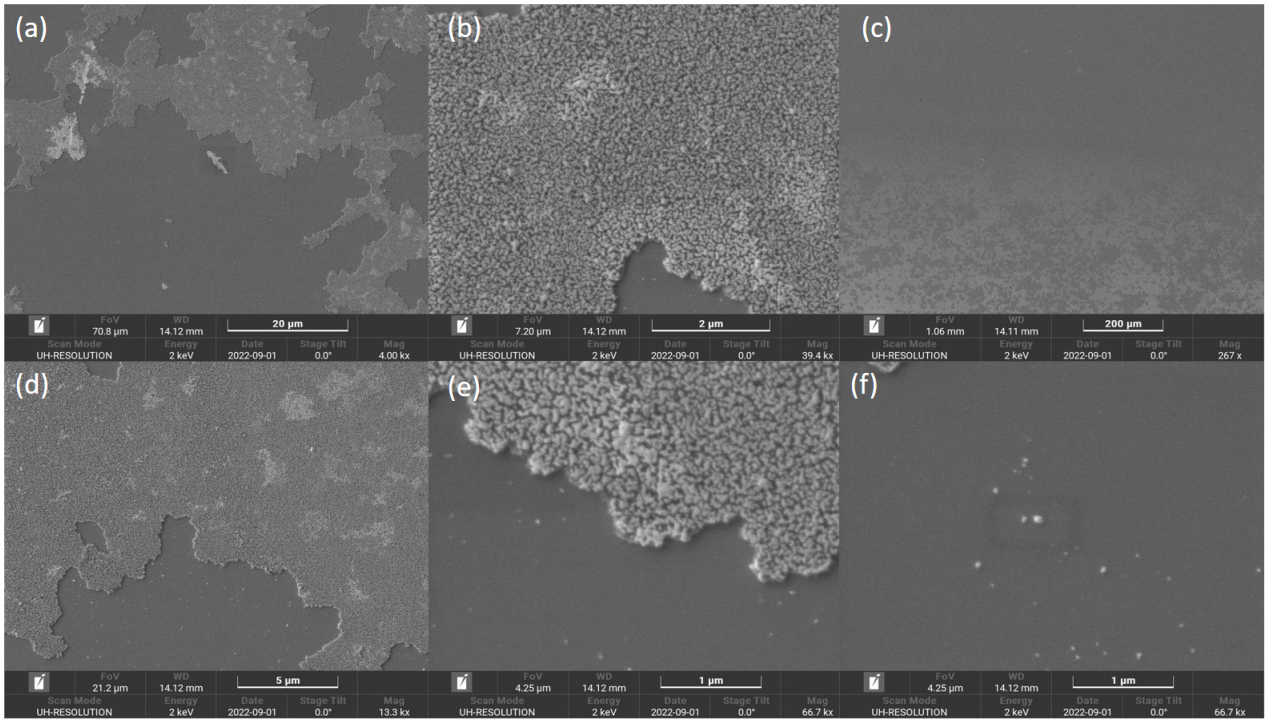

Figure 16: SEM images for sonicated silver sputtered PPs monolayer. (a)View of material not fully sonicated. (b) closer view of unsonicated material. (c) view of interface between spouttered and non sputtered area. (d)-(e) Unsonicated material, (f) remaining polystyrene nanospheres.

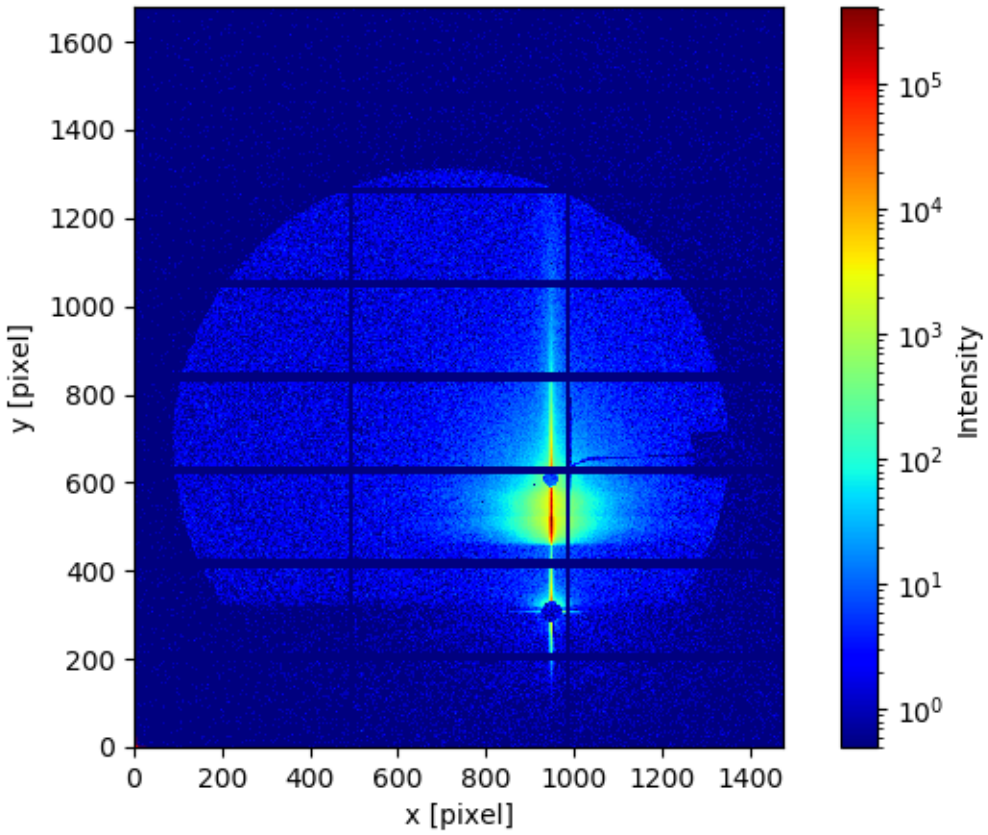

Figure 17: Long exposure taken of silver nanoparticle arrays left after monolayer was sonicated off.

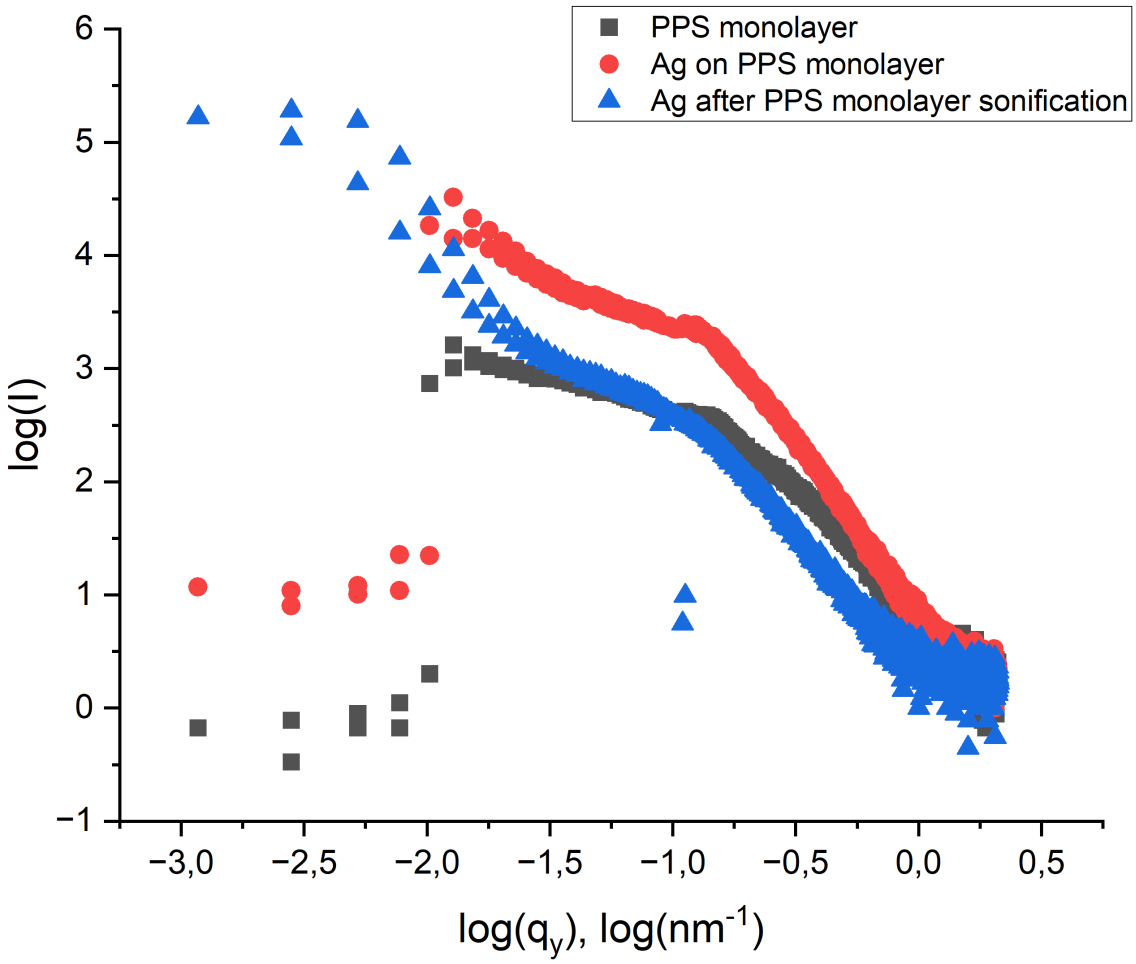

Figure 18: Log graph of linecuts taken for the polystyrene monolayer, the silver sputtered on the polystyrene monolayer and the sonicated silver sputtered polystyrene monolayer.

Appendices

Sample	Diameter (μm)	Surfactant type	Surfactant (%)	Polymer Solution (%)
SE1	4	Methanol	50	50
SE2	4	Methanol	40	60
SE3	3	Methanol	30	70
SE4	3	Methanol	20	80
SE5	4	Methanol	10	90
SE6	3	Methanol	50	50
SE7	3	Methanol	40	60
SE8	3	Methanol	10	90
SE9	3	Methanol	50	50
SE10	3	Methanol	40	60
SE11	2	Methanol	32	68
SE12	2	Methanol	35	65
SE13	2	Methanol	37	63
SE14	3	Ethanol	50	50
SE15	3	Ethanol	40	60
SE16	3	Ethanol	30	70
SE17	3	Ethanol	20	80
SE18	3	Ethanol	10	90
SE19	4	Methanol	99	1
SE20	3	Methanol	99	1
SE21	2	Methanol	99	1
SE22	2	Methanol	35	65
SE23	3	Methanol	50	70
SE24	1.011	Methanol	30	70
SE25	1.011	Methanol	20	80
SE26	0.8	Methanol	30	70
SE27	0.8	Methanol	20	80
SE28	4	Methanol	10	90
SE29	1.011	Methanol	50	50
SE30	1.011	Methanol	40	60
SE31	1.011	Methanol	30	70
SE32	1.011	Methanol	20	80
SE33	1.011	Methanol	10	90
SE34	3	Methanol	40	60
SE35	0.025	Methanol	50	50
SE36	0.194	Methanol	50	50
SE37	0.194	Methanol	40	60
SE38	0.194	Methanol	30	70
SE39	0.194	Methanol	20	80
SE40	0.194	Methanol	10	90
SE41	1.011	Methanol	20	80
SE42	1.011	Methanol	50	50
SE43	1.011	Methanol	10	90
SE44	0.381	Methanol	10	90

Figure 19: Table to show surfactant-polymer solutions produced.

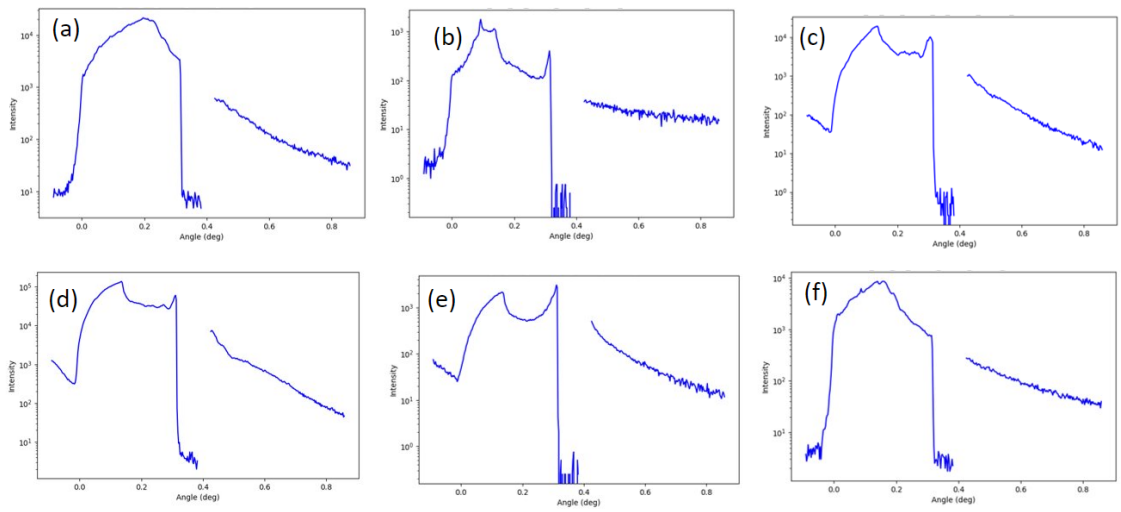

Figure 20: Detector (vertical) linecuts taken from y-scan raw data. (a), (b), (c) are the scans of the silver sputtered on the polymer monolayer half of the wafer, the monolayer half of the wafer and the interface between the two respectively. (d), (e), (f), are the scans of the silver nanoparticle array half of the wafer, the silicon after the monolayer was sonicated off and the interface between the two halves respectively.

Bibliography

[1] H. Gleiter, "Nanostructured materials: Basic concepts and microstructure," *Acta Materialia*, vol. 48, no. 1, pp. 1–29, 2000, ISSN: 1359-6454. DOI: https://doi.org/10.1016/S1359-6454(99)00285-2. [Online]. Available: https://www.sciencedirect.com/science/article/pii/S1359645499002852.

[2] P. Mulvaney, "Surface plasmon spectroscopy of nanosized metal particles," *Langmuir*, vol. 12, no. 3, pp. 788–800, 1996. DOI: 10.1021/la9502711. eprint: https://doi.org/10.1021/la9502711. [Online]. Available: https://doi.org/10.1021/la9502711.

[3] R. M. H. New, R. F. W. Pease, and R. L. White, "Physical and magnetic properties of submicron lithographically patterned magnetic islands," *Journal of Vacuum Science & Technology B: Microelectronics and Nanometer Structures Processing, Measurement, and Phenomena*, vol. 13, no. 3, pp. 1089–1094, 1995. DOI: 10.1116/1.587908. eprint: https://avs.scitation.org/doi/pdf/10.1116/1.587908. [Online]. Available: https://avs.scitation.org/doi/abs/10.1116/1.587908.

[4] S. C. Street, C. Xu, and D. W. Goodman, "The physical and chemical properties of ultrathin oxide films," *Annual Review of Physical Chemistry*, vol. 48, no. 1, pp. 43–68, 1997, PMID: 15012439. DOI: 10.1146/annurev.physchem.48.1.43. eprint: https://doi.org/10.1146/annurev.physchem.48.1.43. [Online]. Available: https://doi.org/10.1146/annurev.physchem.48.1.43.

[5] J. Storhoff, R. Elghanian, R. Mucic, C. Mirkin, and R. Letsinger, "One-pot colorimetric differentiation of polynucleotides with single base imperfections using gold nanoparticle probes," English (US), *Journal of the American Chemical Society*, vol. 120, no. 9, pp. 1959–1964, Mar. 1998, ISSN: 0002-7863. DOI: 10.1021/ja972332i.

[6] G. Pan, R. Kesavamoorthy, and S. A. Asher, "Nanosecond switchable polymerized crystalline colloidal array bragg diffracting materials," *Journal of the American Chemical Society*, vol. 120, no. 26, pp. 6525–6530, 1998. DOI: 10.1021/ja980481a. eprint: https://doi.org/10.1021/ja980481a. [Online]. Available: https://doi.org/10.1021/ja980481a.

[7] S. Sun, C. B. Murray, D. Weller, L. Folks, and A. Moser, "Monodisperse fept nanoparticles and ferromagnetic fept nanocrystal superlattices," *Science*, vol. 287, no. 5460, pp. 1989–1992, 2000. DOI: 10.1126/science.287.5460.1989. eprint: https://www.science.org/doi/pdf/10.1126/science.287.5460.1989. [Online]. Available: https://www.science.org/doi/abs/10.1126/science.287.5460.1989.

[8] J. C. Hulteen, D. A. Treichel, M. T. Smith, M. L. Duval, T. R. Jensen, and R. P. Van Duyne, "Nanosphere lithography: size-tunable silver nanoparticle and surface cluster arrays," *The Journal of Physical Chemistry B*, vol. 103, no. 19, pp. 3854–3863, 1999. DOI: 10.1021/jp9904771. eprint: https://doi.org/10.1021/jp9904771. [Online]. Available: https://doi.org/10.1021/jp9904771.

[9] P. Colson, C. Henrist, and R. Cloots, "Nanosphere lithography: A powerful method for the controlled manufacturing of nanomaterials," *Journal of Nanomaterials*, vol. 2013, Jan. 2013. DOI: 10.1155/2013/948510.

[10] A. Qdemat, E. Kentzinger, J. Buitenhuis, U. Rücker, M. Ganeva, and T. Brückel, "Self assembled monolayer of silica nanoparticles with improved order by drop casting," *RSC Adv.*, vol. 10, pp. 18 339–18 347, 31 2020. DOI: 10.1039/D0RA00936A. [Online]. Available: http://dx.doi.org/10.1039/D0RA00936A.

[11] G. Herzog, G. Benecke, A. Buffet, *et al.*, "In situ grazing incidence small-angle x-ray scattering investigation of polystyrene nanoparticle spray deposition onto silicon," *Langmuir*, vol. 29, no. 36, pp. 11 260–11 266, 2013, PMID: 23927828. DOI: 10.1021/la402254q. eprint: https://doi.org/10.1021/la402254q. [Online]. Available: https://doi.org/10.1021/la402254q.

[12] P. Colson, R. Cloots, and C. Henrist, "Experimental design applied to spin coating of 2d colloidal crystal masks: A relevant method?" *Langmuir*, vol. 27, no. 21, pp. 12 800–12 806, 2011, PMID: 21932793. DOI: 10.1021/la202284a. eprint: https://doi.org/10.1021/la202284a. [Online]. Available: https://doi.org/10.1021/la202284a.

[13] M. Retsch, Z. Zhou, S. Rivera, *et al.*, "Fabrication of large-area, transferable colloidal monolayers utilizing self-assembly at the air/water interface," *Macromolecular Chemistry and Physics*, vol. 210, no. 3-4, pp. 230–241, 2009. DOI: https://doi.org/10.1002/macp.200800484. eprint: https://onlinelibrary.wiley.com/doi/pdf/10.1002/macp.200800484. [Online]. Available: https://onlinelibrary.wiley.com/doi/abs/10.1002/macp.200800484.

[14] C. Zhang, S. Cvetanovic, and J. M. Pearce, "Fabricating ordered 2-d nano-structured arrays using nanosphere lithography," *MethodsX*, vol. 4, pp. 229–242, 2017, ISSN: 2215-0161. DOI: https://doi.org/10.1016/j.mex.2017.07.001. [Online]. Available: https://www.sciencedirect.com/science/article/pii/S2215016117300213.

[15] M. Schwartzkopf and S. V. Roth, "Investigating polymer–metal interfaces by grazing incidence small-angle x-ray scattering from gradients to real-time studies," *Nanomaterials*, vol. 6, no. 12, 2016, ISSN: 2079-4991. DOI: 10.3390/nano6120239. [Online]. Available: https://www.mdpi.com/2079-4991/6/12/239.

[16] D. Meyer, *G i s a x s . d e*, 2022. [Online]. Available: http://www.gisaxs.de/theory.html.

[17] T. Ezquerra, M. Garcia-Gutierrez, A. Nogales, and M. Gomez, *Applications of Synchrotron Light to Scattering and Diffraction in Materials and Life Sciences*, ser. Lecture Notes in Physics. Springer Berlin Heidelberg, 2009, ISBN: 9783540959687. [Online]. Available: https://books.google.de/books?id=QyVqCQAAQBAJ.

[18] M. Schwartzkopf, S.-J. Wöhnert, V. Waclawek, *et al.*, "Real-time insight into nanostructure evolution during the rapid formation of ultra-thin gold layers on polymers," *Nanoscale Horiz.*, vol. 6, pp. 132–138, 2 2021. DOI: 10.1039/D0NH00538J. [Online]. Available: http://dx.doi.org/10.1039/D0NH00538J.

[19] W. Kern, "Chapter 1 - overview and evolution of silicon wafer cleaning technology," in *Handbook of Silicon Wafer Cleaning Technology (Third Edition)*, K. A. Reinhardt and W. Kern, Eds., Third Edition, William Andrew Publishing, 2018, pp. 3–85, ISBN: 978-0-323-51084-4. DOI: https://doi.org/10.1016/B978-0-323-51084-4.00001-0. [Online]. Available: https://www.sciencedirect.com/science/article/pii/B9780323510844000010.

[20] A. Kaliyaraj Selva Kumar, Y. Zhang, D. Li, and R. G. Compton, "A mini-review: How reliable is the drop casting technique?" *Electrochemistry Communications*, vol. 121, p. 106 867, 2020, ISSN: 1388-2481. DOI: https://doi.org/10.1016/j.elecom.2020.106867. [Online]. Available: https://www.sciencedirect.com/science/article/pii/S1388248120302186.

[21] B. Henke, E. Gullikson, and J. Davis, *X-ray interactions: Photoabsorption, scattering, transmission, and reflection at e = 50-30,000 ev, z = 1-92*, 2022.

[22] L. O. Akinsinde, T. E. Glier, M. Schwartzkopf, *et al.*, "Surface characterization and resistance changes of silver-nanowire networks upon atmospheric plasma treatment," *Applied Surface Science*, vol. 550, p. 149 362, 2021, ISSN: 0169-4332. DOI: https://doi.org/10.1016/j.apsusc.2021.149362. [Online]. Available: https://www.sciencedirect.com/science/article/pii/S0169433221004384.